JMEPEG (2011) 20:1188–1195
DOI: 10.1007/s11665-010-9757-3

1059-9495/$19.00

A Study on Factors Influencing Toughness of Basic Flux-Cored Weld of Modified 9Cr-1Mo Steel

B. Arivazhagan and M. Kamaraj

(Submitted February 2, 2010; in revised form July 12, 2010)

Flux-cored arc welding (FCAW) is relatively a new process for joining of modified 9Cr-1Mo (P91) steel. In this study, effect of shielding gas composition, inclusion content, gas tungsten-arc welding (GTAW) surface remelting, and postweld heat treatment (PWHT) on toughness were investigated. The high amount of silicon resulted in the formation of δ-ferrite in basic flux-cored weld. A mixture of 80% argon + 20% (80A) carbon dioxide shielding gas during welding resulted in the required toughness of 47 J at room temperature. The 95% argon + 5% carbon dioxide (95A) gas-shielded welds have lower toughness due to higher amount of δ-ferrite (4%) than 80% argon + 20% carbon dioxide welds (2%). In essence, most desirable shielding gas medium to achieve optimum toughness was 80% argon + 20% carbon dioxide in basic flux-cored arc welding.

Keywords basicity, δ-ferrite, remelting, toughness

1. Introduction

There is a substantial and growing interest in operating thermal power plants at relatively high temperatures (~600°C) and/or pressures (~350 bar) for improving thermal efficiency and reducing carbon dioxide emissions. Materials with a ferritic/martensitic microstructure are preferred to austenitic stainless steels because of their superior properties such as good thermal conductivity, low coefficient of thermal expansion, coupled with higher resistance to thermal shock, low oxidation rate, and excellent weldability. Orlova et al. (Ref 1) highlighted the importance of high-Cr ferritic steels as a good replacement for exiting low-Cr ferritic steels (P11 and P5) in power plant applications. For these reasons, there has been a growing demand for the development and application of several kinds of 9-12% chromium steels (Ref 2).

Among these, the modified 9Cr-1Mo steel (ASTM A387 Grade91) has found increased application over the recent years within the power generation industry. It has been employed not only for the repair and upgrade of existing plant but also in the construction of new plant (Ref 3). It has been used for headers in steam power plant, tubing for heat exchangers, major thick section pressure parts of the boiler, turbine, and also in the high-temperature energy options, viz., fossil, solar, thermal, nuclear fusion systems, and fast breeder steam generator components (Ref 4). Apart from this, the substitution of 9Cr-1Mo steels for certain applications will constitute significant conservation of both Cr and Ni (Ref 5).

B. Arivazhagan and **M. Kamaraj**, Department of Metallurgical and Materials Engineering, Indian Institute of Technology, Madras, Chennai 600 036, India. Contact e-mail: chengaiari@yahoo.co.in.

The improvement in high temperature creep strength of these materials is achieved by the addition of controlled levels of niobium, vanadium, and nitrogen to a conventional 9Cr-1Mo (P9) base composition (Ref 6). This leads to the development of a dispersion of fine Nb carbonitrides precipitated during the tempering heat treatment, and also the formation of stable precipitates containing vanadium within the subgrains (Ref 7). The $M_{23}C_6$ carbides form mainly at the interfaces of austenite grains and martensite laths. They retard the subgrain growth whereas carbonitrides pin free dislocations leading to enhanced creep strength of the material (Ref 8).

Welding is the major fabrication process for most of the high-temperature components. Although P91 is weldable without cracking of any kind, there are two problems related to welding, which cause concern: joint creep strength and weld fusion zone toughness. The weld metal toughness may be thought to be irrelevant in assemblies designed for operation in the temperature range of 500-600 °C, since this is far in excess of the temperature range at which brittle fracture occurs. However, the components may very well also be stressed at ambient temperature during pressure testing or start-up, for example. To minimize the possibility of brittle fracture in these situations, a minimum average of 47 J for the tempered weld metal (minimum single value of 38 J) at room temperature (20 °C) has to be ensured as per the European specification EN1599:1997 (Ref 9).

Proper selection of filler material and its composition plays a major role in deciding the soundness of the weld. The advantages of P91 steel can only be fully exploited provided these steels can be welded with appropriate welding consumables to ensure that weldments possess acceptable properties. The weld deposit is designed to conform as close as possible to the composition of the parent steel, with consistency in achieving optimum properties and weldability. However, later studies based on the earlier specification showed that the toughness of the weld metal proved to be rather low after tempering. It is therefore necessary to change the weld metal composition to be different from that of the parent metal,

particularly for the flux-shielded welding processes such as shielded metal arc welding (SMAW) and submerged arc welding (SAW) to ensure a sound weld. Dittrich et al. (Ref 10) in their research have shown that reduction in niobium, nitrogen, and silicon contents in weld improves toughness, whereas increased nickel content can be beneficial. However, the nickel + manganese content has to be adjusted such that the A_{C1} temperature does not fall below the postweld heat treatment (PWHT) temperature (Ref 8). The need to balance filler material composition to restrict the occurrence of δ-ferrite and also to ensure a fully martensitic structure in the fusion zone has also been highlighted by Sireesha et al. (Ref 11) in their studies on joining of P91 steel. Both SMAW and SAW employ basic flux systems exclusively to reduce the oxygen potential and hence the inclusion content to improve toughness (Ref 12).

During the last 5 years, flux-cored arc welding (FCAW) has also made its advent, and FCAW electrodes for joining P91 are now commercially available. The use of flux-cored wire offers significant benefits in terms of increased productivity, welder appeal, reduced fabrication time, and costs. The advantage of a higher deposition rate is particularly notable for positional welding (Ref 13). However, in order to ensure desirable welding characteristics (smooth weld metal transfer, flat weld bead profiles, and easy slag removal), FCAW process has to employ a rutile-based flux system instead of the otherwise more desirable basic system (Ref 13). Arivazhagan et al. (Ref 14) studied that in rutile flux-cored P91 steel welds, the oxygen and inclusion contents are higher, and, hence, the fusion zone toughness was correspondingly lower than 47 J at room temperature. There is a need to improve the toughness of P91 steel welds to maintain a toughness of more than 47 J. Basic flux system is another option to meet the toughness requirement. In this study, shielding gas composition is varied to study its influence on basic FCAW process parameters, microstructural variations, and fusion zone toughness.

Table 1 Chemical composition of P91 base metal, wt.%

C	Mn	P	S	Si	Cr	Mo	V	Nb	Ni
0.08	0.39	0.02	0.01	0.50	9.4	1.0	0.25	0.09	0.13

Table 2 Mechanical properties at room temperature

Yield strength, MPa	Tensile strength, MPa	Elongation, %	Impact energy, J
557	672	18	227

2. Experimental Work

The base material used in this study was a modified 9Cr-1Mo (P91) steel plate in the normalized (1080 °C for 1 h) and tempered (760 °C for 2 h) conditions. Its chemical composition (wt.%) as evaluated by optical emission spectroscopy, and mechanical properties at room temperature are summarized in Table 1 and 2, respectively.

For welding, the P91 steel plate was cut into size of 220 × 110 × 12.5 mm by plasma arc cutting followed by machining processes such as milling and surface grinding. The dimensions of weld geometry were a root opening of 2.4 mm, a root face of 1.2 mm, and an included single V-groove angle of 60°. A seamless 1.2-mm diameter basic flux-cored wire (as per AWS A5.29 specification) was used in the trials for the filler passes with root layer completed by gas tungsten-arc welding (GTAW: EWTh-2) process using a 2.4-mm diameter rod. Four types of shielding gases (designation in brackets used hereafter in the text) were used in the trials: pure argon (A), pure carbon dioxide (C), premixed shielding gases 80% argon + 20% carbon dioxide (80A), and 95% Argon + 5% CO_2 (95A). An inverter-based power source was used for welding trials (DCEP) and deposition was completed in flat (1G) position. Preheat (200 °C) and interpass (250 °C) temperatures were maintained using oxy-acetylene (neutral flame) torch and monitored using thermal chalks. Welding parameters were optimized after extensive trails, which are summarized in Table 3. After welding, the joints were radiographed in accordance with ASME Sect II-article 2, and those passing the inspection were given a PWHT at 760 °C for various durations (2 and 5 h) in a muffle furnace. Autogenous GTAW surface remelting was done on the final layer of the weldment, in a weaving mode to a width equal to the width of the final layer at a heat input of 14 kJ/mm.

Transverse cross sections of the sound weld joint for optical microstructural examination were prepared by standard metallographic procedures etched with Vilella's reagent consisting of 1 g picric acid, 5 mL HCl, and 100 mL alcohol. Scanning electron microscopy (SEM) and transmission electron microscopy (TEM) were used for the examination of microstructure in detail. Energy-dispersive x-ray spectrometry (EDS) analysis of the phases present in the weld metal was also conducted. TEM study was performed on the section parallel to the fusion zone using thin foils prepared by mechanical polishing followed by twin-jet electro polishing using an electrolyte consisting of a mixture of 80% methanol and 20% perchloric acid, which was held at a temperature of −30 °C. For toughness evaluation as per ASTM E-23, Charpy specimens of size 55 × 10 × 10 mm were cut from the transverse cross section of joints, with the notch located in the weld fusion zone and oriented parallel to the welding direction. Five specimens were tested at

Table 3 Welding parameters

Process	Number of layers	Welding current, A	Welding voltage, V	Heat input, kJ/mm
FCAW(a)	Three	180	24	1.4
GTAW	Root layer	110	24	1.0
GTAW remelting process	Single pass in weaving mode	200	26	14

(a) Total number of passes: five

each condition; the reported energy is an average of three intermediate values, leaving out the maximum and minimum values of energy.

3. Results and Discussion

3.1 Welding Characteristics

Initial trials were carried out using FCAW process alone. This resulted in large amount of slag entrapment at the root and also in other layers as observed in radiograph of joints. Visual inspection before each layer deposition during welding has not revealed any slag layer on top of the weld. Radiographic examination revealed the presence of slag. This was due to entrapment of slag in the molten weld pool during deposition. Variation in heat input (from 1.4 kJ to 2.2 kJ/mm) during welding has not removed the slag entrapment. Slag entrapment can be successfully avoided by depositing the root layer by GTAW process. With pure argon shielding, more amount of slag entrapped throughout the weldment. Arivazhagan et al. (Ref 14) in their studies on rutile FCAW of P91 steel, observed same kind of slag entrapment in rutile FCAW process. Hence further trials were carried out with GTAW root layer in the joint. Pure carbon dioxide (C) shielding generated large amount of spatter. Shielding gases, namely, 80A and 95A generated least amount of spatter during welding. In general, spatter generation was observed during welding. This is due to unstable arc associated with use of basic flux in the wire (Ref 15). After completion of each pass, a thick, brittle slag layer was formed on the bead. The slag was removed by repeated peening on the surface. Shielding gas composition variation has not changed the thickness of slag layer. Weld pads were prepared using 80A and 95A shielding gases each to study the influence of shielding gas composition on toughness.

3.2 Slag Analysis

In order to identify the basicity of flux in the filler wire, the slag was removed from the joint area after welding, crushed into fine powder, and subjected to composition analysis by x-ray fluorescence (XRF) technique. Figure 1 shows the (XRF) profile of slag produced after welding. Table 4 summarizes the chemical composition (wt.%) of slag by XRF method.

Morigaki et al. (Ref 16) developed an empirical relation known as Mori index for identification of basicity index (BI) of flux based on chemical composition of slag. The composition in wt.% was converted into mole fraction for substitution in Mori index. Using Mori index, BI of flux was evaluated. Slags arc basic when BI is positive, and acidic when it is negative, while neutral fluxes have a BI value close to zero. The empirical relation is as follows:

$$\mathrm{BI} = 6.05\mathrm{CaO} + 4.8\mathrm{MnO} + 4.0\mathrm{MgO} + 3.4\mathrm{FeO} - (6.31\mathrm{SiO_2} + 4.79\mathrm{TiO_2} + 0.2\mathrm{Al_2O_3}) \quad \text{(Eq 1)}$$

Substituting the values, the BI value was positive, which indicates that the flux belongs to basic type.

3.3 Chemical Composition of Welds

The chemical compositions of the diluted weld metals are summarized in Table 5. There are various empirical relations available to predict the formation of δ-ferrite in the welds (Ref 17). Among these relations, Schneider formula is widely used to predict the formation of δ-ferrite based on the composition of welds. The possibility of ferrite formation can be predicted based on ferrite factor (FF). The ferrite factor is defined as the difference between chromium equivalent (Cr_{eq}) and Nickel equivalent (Ni_{eq}) values.

To obtain weld metals with fully martensitic structure, it appears necessary to consider a Schneider Cr_{eq} value of lower than 13.5 and the difference between the chromium and nickel equivalents i.e., FF to be lower than a value of 8. The Schneider formula is as follows:

$$\mathrm{Cr_{eq}} = \mathrm{Cr} + 2\mathrm{Si} + 1.5\mathrm{Mo} + 5\mathrm{V} + 1.75\mathrm{Nb} + 0.75\mathrm{W} \quad \text{(Eq 2)}$$

$$\mathrm{Ni_{eq}} = \mathrm{Ni} + 0.5\mathrm{Mn} + 30\mathrm{C} + 25\mathrm{N} + 0.3\mathrm{Cu} \quad \text{(Eq 3)}$$

In this study, based on the Cr_{eq} and Ni_{eq} values, and FF, the formation of δ-ferrite in the weld is possible. As the oxidizing

Table 4 Chemical composition of basic slag

Slag	CaO	MnO	MgO	FeO	SiO_2	TiO_2	Al_2O_3
Basic, wt.%	72.27	3.96	0.04	2.71	2.09	12.54	0.28
Mole fraction	0.874	0.038	0.001	0.026	0.023	0.036	0.002

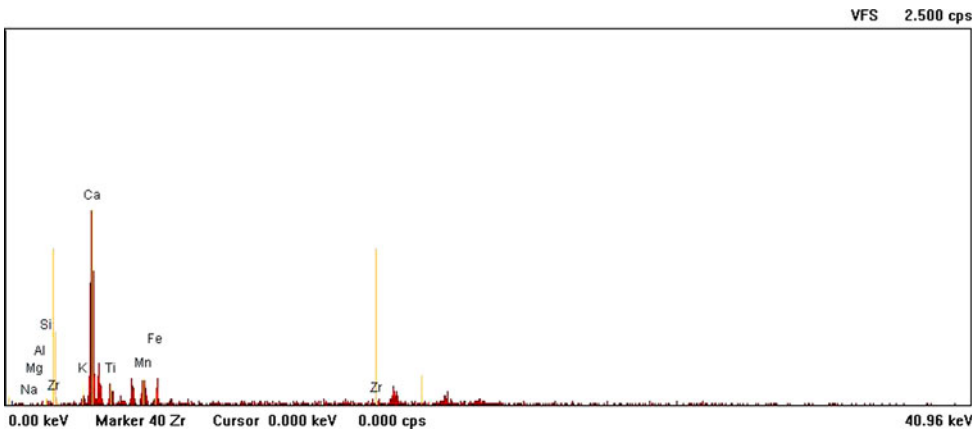

Fig. 1 XRF profile of basic flux-cored arc weld slag

Table 5 Chemical composition basic flux-cored arc weld metals, wt.%

Weld	C	Mn	Si	Cr	Mo	V	Nb	Ni	Oxygen, ppm	FF
A	0.11	0.56	0.46	9.18	1.00	0.24	0.06	0.29	450	9.03
95A	0.12	0.71	0.46	9.65	0.94	0.24	0.07	0.29	480	9.06
80A	0.12	0.68	0.32	9.73	1.04	0.23	0.07	0.25	520	9.01
C	0.11	0.59	0.32	8.90	1.13	0.21	0.05	0.29	650	8.49
GTAW melt of 80A	0.10	0.68	0.30	9.65	1.1	0.22	0.06	0.25	535	10.51

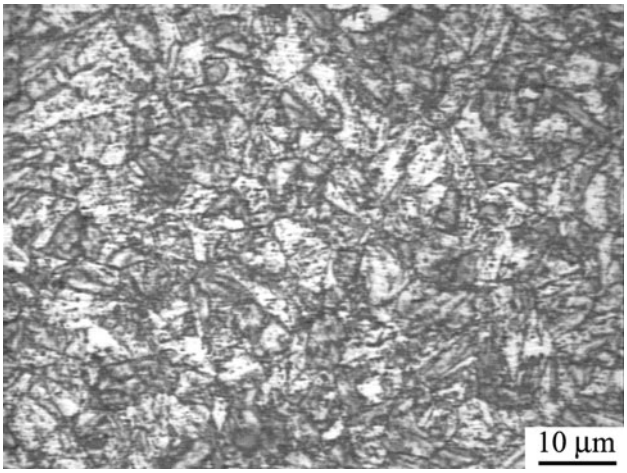

Fig. 2 Optical image of tempered martensite

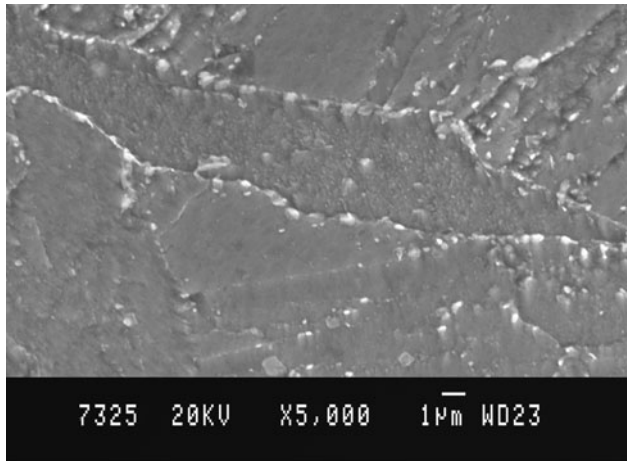

Fig. 3 SEM image of tempered martensite

component of the shielding gas increases, there was an increase in the oxygen content of the welds. Mn, Si, Cr, V, and Nb contents were significantly affected due to the increase in carbon dioxide content of the shielding gas. This has been attributed to loss of alloying elements by oxidation, and formation of inclusions with increase in the oxygen content of shielding gas. The lower critical temperature (A_{C1}) of welds was empirically found using the equation.

$$A_{C1} = 801 + (\mathrm{Ni} + \mathrm{Mn}) + 0.4(\mathrm{Ni} + \mathrm{Mn})^2 \quad \text{(Eq 4)}$$

where temperature is in °C and composition is in wt.% (Ref 18). Experimental data suggest that the expression may underestimate (A_{C1}) at the higher levels of (Ni + Mn). The PWHT temperature should be less than the (A_{C1}) temperature to avoid the formation of fresh untempered martensite formed during cooling. In this study, the PWHT temperature (760 °C) used was less than the A_{C1} (800 ± 1.5 °C) as predicted by the equation.

3.4 Microstructure

The microstructure of the normalized and tempered base material is presented in Fig. 2.

The optical micrograph shows a tempered martensite, with the prior austenite grain boundaries being well outlined by the precipitates of mainly $Cr_{23}C_6$ type formed during tempering.

The SEM micrograph, Fig. 3, shows the distribution of precipitates within the grains and also at grain boundaries at a higher magnification (5000×).

The TEM micrograph in Fig. 4 shows lath martensite with discontinuous precipitation along the lath boundaries and also a few cuboidal precipitates within the laths.

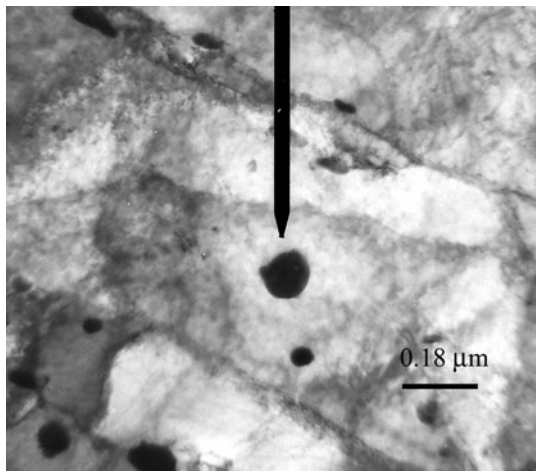

Fig. 4 TEM image of lath martensite in normalized and tempered condition in base metal

The latter have been identified by TEM-EDS analysis (Fig. 5) to be niobium carbide and its composition (wt.%) is as follows: V = 1.3, Cr = 3.5, Fe = 31.9, and Nb = 63.4.

These carbonitride precipitates are essential in enhancing the creep strength of steel. The unetched SEM images (Fig. 6-8) show the size and distribution of microinclusions in welds. As the CO_2 content in the shielding gas mixture increases, there was increase in quantity of microinclusion in welds. The inclusion populations estimated using the image analysis results are summarized in Table 6.

The coarse microinclusions (> 5 µm) are observed in only pure carbon dioxide-shielded (C) welds. Other shielding gases

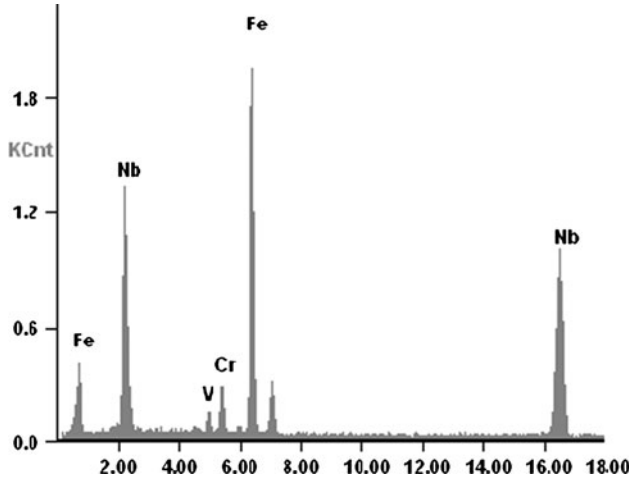

Fig. 5 EDS analysis of carbonitride precipitate

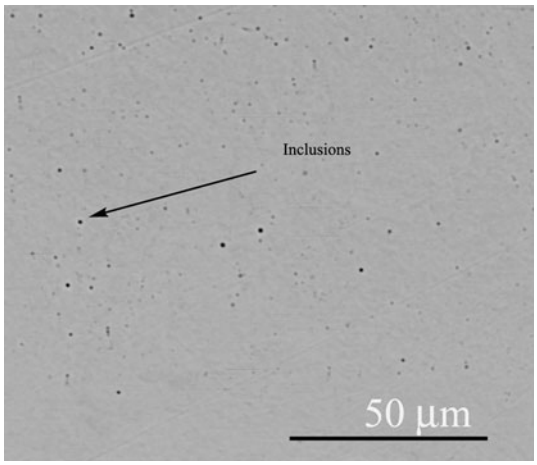

Fig. 6 BSE image showing presence of fine microinclusions in '95A' weld

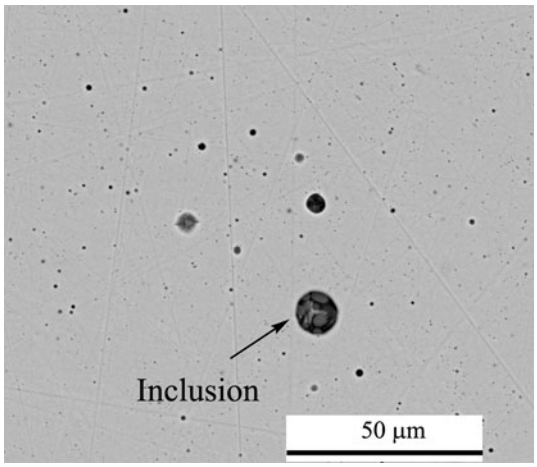

Fig. 7 BSE image of 'C' weld having microinclusions with various size

produce welds with fine inclusions. The coarse microinclusions are observed in pure carbon dioxide-shielded welds despite the basic flux in the wire. This has been due to a greater amount of

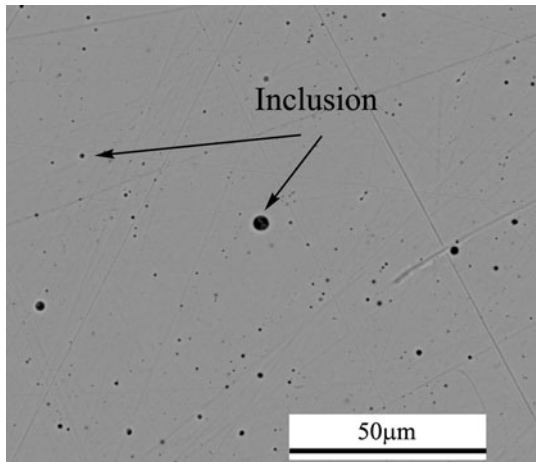

Fig. 8 BSE image of '80A'-shielded weld showing microinclusions

Table 6 Microinclusion characteristics in a basic weld

Weld	Fine inclusion (2-5 µm)	Coarse inclusion (>5 µm)	Mean distance between inclusions, µm
95A	30	Nil	30
80A	50	Nil	25
C	100	2	20
GTAW remelt of 80A	55	Nil	22

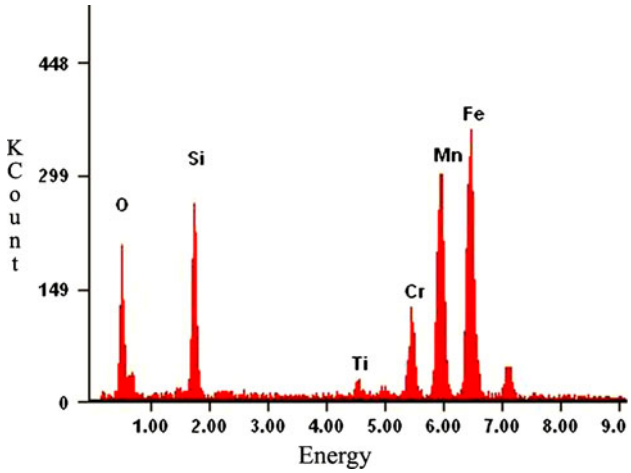

Fig. 9 EDS analysis of a microinclusion in weld

oxygen in the arc atmosphere as a result of using pure carbon dioxide shielding gas during welding. The inclusions are nearly spherical in shape, and they are rich in silicon, manganese, and oxygen (Fig. 9).

A typical composition (wt.%) of an inclusion as revealed by EDS analysis is as follows: O = 13.80; Si = 11.40; Mn = 28; Fe = 35; Cr = 9.50; and Ti = 1.70. The Optical image of as-welded microstructure (Fig. 10) shows faint prior austenite grain boundaries due to the absence of precipitate formation.

In the as-welded condition, the micrograph clearly shows the presence of δ-ferrite. This was obviously due to higher

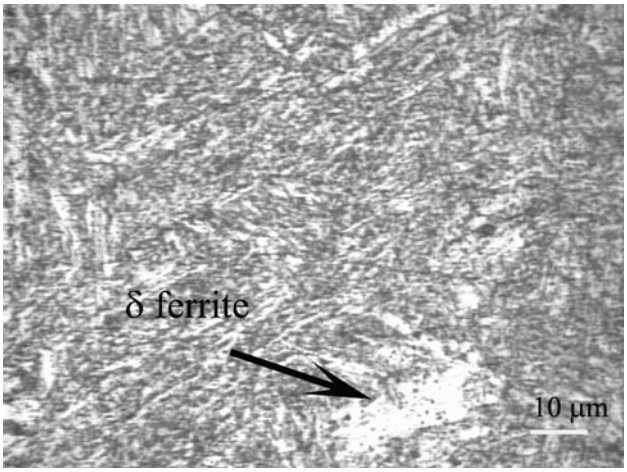

Fig. 10 Optical as-welded microstructure showing the presence of δ-ferrite in martensite matrix

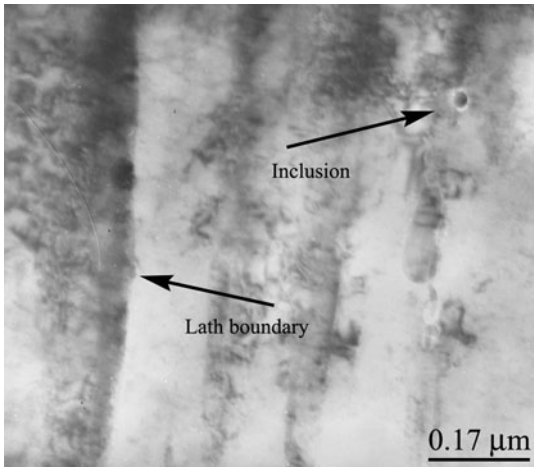

Fig. 11 TEM image of lath martensite in as-welded condition

silicon content (>0.30), being a strong ferrite stabilizer, compared with rutile flux-cored welds (<0.30) (Ref 14). Arivazhagan et al., reported in their studies on rutile FCAW of P91 steel that there was no δ-ferrite in welds. In 80A-shielded welds, the δ-ferrite content was 1.81% with isolated morphology located within the grains. In 95A-shielded welds, with increase in silicon content (0.46%), the net ferrite content was 4%. Apart from the composition, cooling rate also has significant influence on the formation of δ-ferrite in weld. A high cooling rate leads to more amount of δ-ferrite retention than slow cooling rate (Ref 11). TEM image of (Fig. 11) as-welded microstructure shows lath martensite with dislocation network.

At a higher magnification, TEM image (Fig. 12) of the as-welded microstructure shows randomly oriented Fe-Cr rich needles in the untempered martensite.

Dislocation networks are observed in the microstructure. The needles are approximately 0.5 μm in length with width being 0.05 μm. Only needle-like precipitates are observed in the as-welded condition. These needle structures are formed due to auto-tempering of welds during multipass welding. The composition (wt.%) of needle-like precipitate as revealed by EDS analysis (Fig. 13) is as follows: Cr = 29.90; and Fe = 70.10.

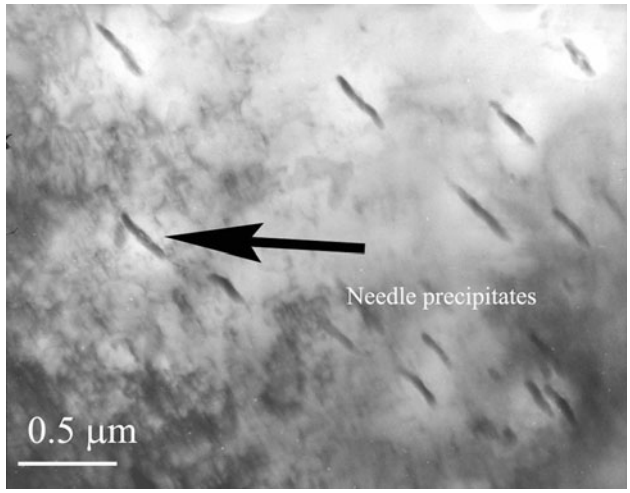

Fig. 12 TEM image of as-welded microstructure showing the presence of needle-like precipitates

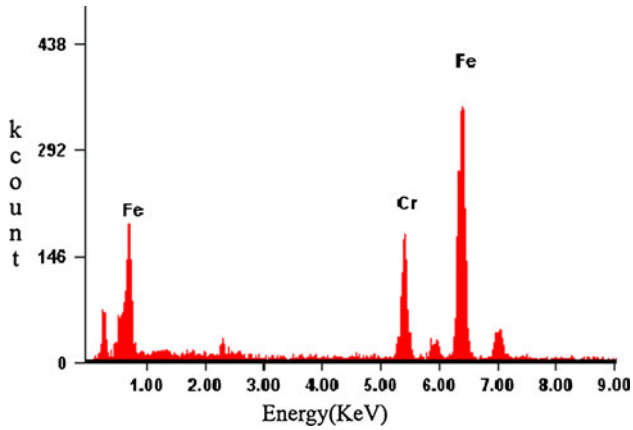

Fig. 13 EDS analysis of needle-like precipitate in weld

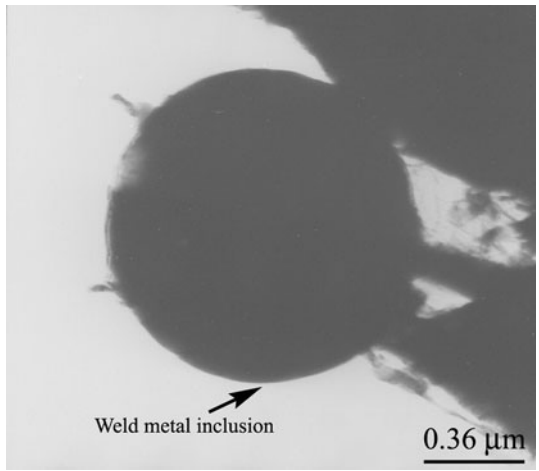

Fig. 14 Typical weld metal inclusion in a basic weld

The inclusions are (Fig. 14) spherical in shape. The TEM image of weld after PWHT at 760 °C-2 h shows (Fig. 15) predominately Cr-rich precipitate at the lath boundaries.

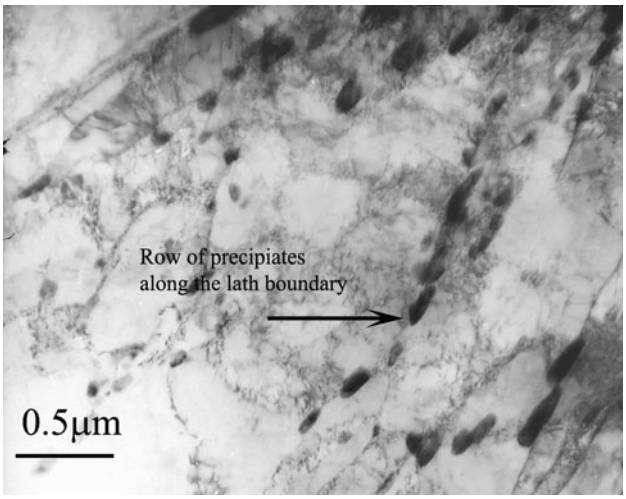

Fig. 15 Tempered weld microstructure (760 °C for 2 h)

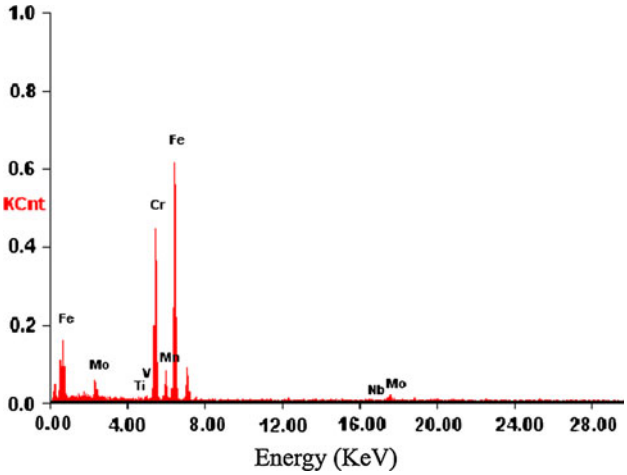

Fig. 16 EDS analysis of carbonitride precipitate at the lath boundary

Subgrain formation is also clearly noticed. The Cr-rich precipitates vary in shape and size. They are belonging to $Cr_{23}C_6$ type as indicated by EDAX (Fig. 16) analysis. The EDS analysis of carbonitride precipitate is as follows: Cr = 30.4; Mo = 3.8; V = 0.5; Nb = 0.4; Mn = 0.7; and Si = 0.5. A few carbonitrides rich in vanadium and niobium also observed.

3.5 Toughness of Welds

The Charpy V-notch impact energy of welds at room temperature is listed in Table 7.

The toughness in the as-welded condition is found to be low due to the presence of needle-like precipitates in the untempered martensite matrix. These needle-like precipitates act like brittle notches in the weld, hence cause low toughness. After PWHT, toughness improved significantly, owing to microstructural changes such as reduced dislocation density, subgrain formation, and replacement of needle-like precipitates by other forms of precipitates in tempered martensite. In this study, it is observed that the presence of δ-ferrite (2%) does not affect the toughness of weld in 80A-shielded welds. This has been due to the morphology of ferrite i.e., isolated islands of ferrite as

Table 7 Toughness (J) of basic flux-cored arc welds at 30 °C

Weld	760 °C for 2 h	760 °C for 5 h
95A	27	43
80A	57	68
GTAW remelted 80A weld	62	72

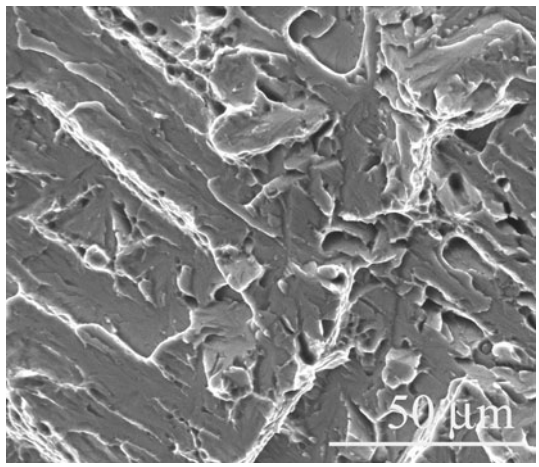

Fig. 17 SEM fractograph in as-welded (80A) condition showing cleavage fracture

shown in Fig. 10. Onoro observed that this morphology of ferrite is less harmful compared with other forms of ferrite such as intergranular ferrite, and polygonal ferrite (Ref 17). The low volume fraction (0.08) of inclusions with less harmful nature of ferrite morphology improves the toughness of 80A-shielded welds. In the case of 95A-shielded welds, the volume fraction of ferrite (4%) increases because of the higher amount of silicon content (Si = 0.46%) than in 80A-shielded welds (Si = 0.32%). The higher amount of δ-ferrite reduced the toughness of 95A-shielded welds drastically compared with 80A-shielded welds. Though the volume fraction of inclusion is less, the higher amount of δ-ferrite reduced the toughness significantly. Even after PWHT at 760 °C for 5 h, the toughness was not improved to a great extent. This is obviously due to significant influence of ferrite content than inclusion content on toughness. In this study, there was some marginal improvement in the toughness of GTAW-remelted welds compared with unmelted welds. The reason is as follows: the GTAW remelting was effective only in the case of welds containing coarser microinclusions (>5 μm) (Ref 14). From this study, it was inferred that GTAW remelting was effective in case of welds containing fine microinclusions only since there is not much change in inclusion content after remelting and also in toughness data.

3.6 Fractography

SEM examination of Charpy fracture surface in the as-welded condition shows (Fig. 17) cleavage fracture due to low toughness (10 J) caused by needle-like precipitates.

The fracture is flat with featureless surface. This is due to high hardness (400 VHN) that is associated with untempered martensite. After PWHT at 760 °C for 2 h, the fracture surface of welds (Fig. 18) shows ductile mode of fracture due to

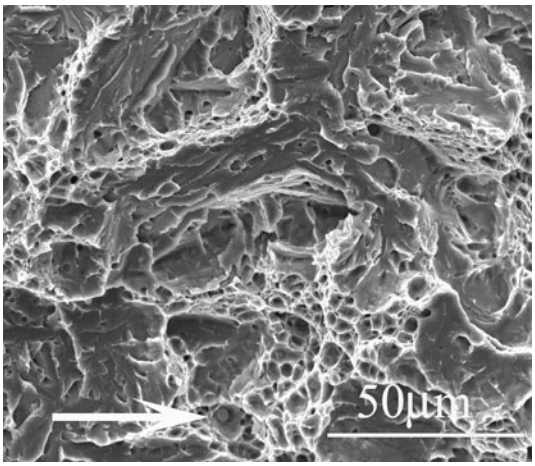

Fig. 18 SEM fractograph of weld (80A) after PWHT at 760 °C for 2 h showing mixed mode of fracture

reduction in hardness (278 VHN) and also microstructural changes induced by the tempering process. The dimples are fine in size, and a few of the dimple cavities contain inclusions as shown in Fig. 18.

The 95A-shielded weld fractograph shows cleavage fracture due to the presence of δ-ferrite. As the postweld duration increases, there is an increase in dimple content of welds due to reduction in strength of the matrix.

4. Conclusions

(1) In the flux-cored arc welding (FCAW), the slag entrapment at the root layer can be avoided by using GTAW process for root-pass deposition.
(2) GTAW-remelting process was an effective technique to refine the coarse microinclusions content in weld to improve the toughness. After GTAW surface melting, basic welds show 8% increase in the toughness of welds.
(3) As the PWHT duration increases, there is a continual improvement in the toughness of welds.
(4) δ-Ferrite is observed in 80% argon + 20% CO_2 (2% δ-ferrite)- and 95% + 5% CO_2 (4% δ-ferrite)-shielded basic flux-cored arc welds. When the δ-ferrite content is above 2%, the toughness falls below the required 47 J.
(5) A basic flux-cored wire having silicon content of 0.32% higher than the specified limit of standards (0.30%) can meet the toughness requirement satisfactorily. This is due to the efficient deoxidation associated with high amounts of deoxidizers such as SiO_2 and MnO in the flux and also the less-harmful variant of δ-ferrite (isolated islands of δ-ferrite) that is present within the grains of weld. In basic flux-cored wire, high amounts of Nb (0.07%), V (0.23%), and Si (0.32%) can be tolerated without affecting the toughness significantly as observed in this study. At a silicon level of 0.46%, the weld fails to meet the toughness requirement of 47 J.
(6) In basic FCAW process, ideal shielding gas combination to achieve the desired toughness is that of 80% argon + 20% CO_2.

References

1. A. Orlova, J. Bursik, K. Kucharova, and V. Sklenicka, Evolution of Microstructure in P91-Type Steel in High Temperature Creep, *Microstructural Stability of Creep Resistant Alloys for High Temperature Applications*, A. Strang, Ed., The Institute of Materials, London, 1998, p 89–106
2. H. Cerjak and E. Letofsky, The Effect of Welding on the Microstructural Development of Advanced 9-12 Cr Steels, *Microstructural Stability of Creep Resistant Alloys for High Temperature Applications,*, A. Strang, Ed., The Institute of Materials, London, 1998, p 323–338
3. A.M. Barnes, The Effect of Composition on Microstructural Development and Mechanical Properties of Modified 9%Cr1%Mo Weld Metals, *Microstructural Stability of Creep Resistant Alloys for High Temperature Applications*, A. Strang, Ed., The Institute of Materials, London, 1998, p 339–360
4. R.W. Vanstone, The Contribution of Microstructural Investigations to the Development of Improved Materials for Future High Temperature Steam Turbines, *Microstructural Stability of Creep Resistant Alloys for High Temperature Applications*, A. Strang, Ed., The Institute of Materials, London, 1998, p 457–470
5. G.W. Cunningham, P. Patriarca, and E.E. Hoffman, Ferritic Steels as Alternate Structural Materials for High Temperature Applications, *Microstructural Stability of Creep Resistant Alloys for High Temperature Applications*, A. Strang, Ed., The Institute of Materials, London, 1983, p 3–8
6. W.H. Lee, R.K. Shiue, and S.C. Chen, Mechanical Properties of Modified 9Cr-1Mo Steel Welds with Notches, *Mater. Sci. Eng. A*, 2003, **356**, p 153–161
7. W.B. Jones, C.R. Hills, and D.H. Polonis, Microstructural Evolution of Modified 9Cr-1Mo Steel, *Metall. Trans. A*, 1991, **22A**, p 1049–1058
8. A. Barnes, The Influence of Composition on Microstructural Development and Toughness of Modified 9% Cr-1Mo Weld Metals, TWI Report, 509/1995, 1995
9. E.-L. Bergquist, Consumable and Welding Modified 9Cr-1Mo Steel, *Svetsaran*, 1999, **1–2**, p 22–25
10. S. Dittrich, V. Gross, and H. Heuser, Optimized and Advanced P (T) Filler Metals, *National Welding Seminar*, IIW, Jamshedpur, 1994, p 4R2/1–4R2/4
11. M. Sireesha, S.K. Albert, and S. Sundaresan, Microstructure and Mechanical Properties of Weld Fusion Zones in Modified 9Cr-1Mo Steel, *J. Mater. Eng. Perform.*, 2001, **10**(3), p 320–330
12. I.E. French and M.R. Bosworth, A Comparison of Pulsed and Conventional Welding with Basic Flux Cored and Metal Cored Welding Wires, *Weld. J.*, 1995, **74**, p 197s–205s
13. Z. Zhang, A.W. Marshall, and G.B. Holloway, Flux-Cored Arc Welding: High Productivity Welding Process for P91 Steels. *EPRI Conference on 9Cr Materials Fabrication and Joining Technology*, USA, 2001, p 1–14
14. B. Arivazhagan et al., Effect of TIG Arc Surface Melting Process on Weld Metal Toughness of Modified 9Cr-1Mo (P91) Steel, *Mater. Lett.*, 2008, **62**(17–18), p 2817–2820
15. S. Kou, *Welding Metallurgy*, 2nd ed., Wiley Interscience, New York, 2003, p 54–59
16. O. Morigaki, T. Matsumoto, T. Yoshida, and M. Makita, International Institute of Welding, Document No. XII-13-134-73, 1973
17. J. Onoro, Martensite Microstructure of 9-12% Cr Steel Weld Metals, *J. Mater. Process. Technol.*, 2006, **180**, p 137–142
18. R.W. Swindeman, M.L. Santella, P.J. Maziasz, B.W. Roberts, and K. Coleman, Issues in Replacing Cr-Mo Steels with 9Cr-1Mo-V Steel, *Int. J. Press. Vessels Piping*, 2004, **81**, p 507–512